*36th EPS Conference on Plasma Phys. Sofia, June 29 - July 3, 2009 ECA Vol.**33E**, P-4.115 (2009)*

Gyrokinetic Simulations Of Electron Scale Turbulence In Spherical Tokamak Plasmas With Flow Shear

W. Guttenfelder[1], R.J. Akers[2], J. Candy[3], A.R. Field[2], A.G. Peeters[1], C.M. Roach[2]

[1]*Centre for Fusion, Space & Astrophysics, Department of Physics, University of Warwick, Coventry CV4 7AL, UK*

[2]*EURATOM/UKAEA Fusion Association, Culham Science Centre, Abingdon, OX14 3DB, UK*

[3]*General Atomics, San Diego, California 92121, USA*

While measured ion thermal transport in spherical tokamaks (STs) such as MAST can approach the level of neoclassical theory [1], electron thermal transport is almost always anomalous. The large levels of E×B shear often observed in STs are expected to suppress the turbulent transport driven by ion scale ($k_\perp\rho_i \leq 1$) ion temperature gradient (ITG) and trapped electron mode (TEM) instabilities. However, both non-linear turbulence simulations [2,3] and 1D transport modeling [4,5] predict electron scale turbulence ($k_\perp\rho_e \leq 1$) driven by the electron temperature gradient (ETG) can drive experimentally relevant levels of transport. Analysis of recent discharges in NSTX suggest that microtearing instabilities [6] and even energetic particle driven transport [7] may be the dominant electron thermal transport mechanism for higher NBI heating power (P_{NBI}=4-6 MW).

Here we attempt to quantify the ETG transport in MAST discharges with heating power $P_{NBI} \leq 2$ MW. Nonlinear gyrokinetic simulations are performed using GYRO [8] for low-aspect ratio, moderately shaped equilibrium defined by the Miller parameterization (R/a=1.6, r/a=0.5, κ=1.5, δ=0.2). The safety factor, q, and corresponding magnetic shear, $\hat{s}$, approach large values in the outer half of ST plasmas ($\hat{s} \sim 2-6$). Previous ETG simulations using the adiabatic ion model (ETG-ai) [2] indicate a lack of saturation for $\hat{s} > 0.4$ when including particle trapping. Evidently, including gyrokinetic ions [2], finite E×B shear [9], or electron collisionality [10] provides a long-wavelength cutoff that recovers a saturated turbulent state. To ensure saturation and convergence for ST parameters, the simulations here ($q=1.4, \hat{s}=0.8$) include both gyrokinetic ions (m_i/m_e=3600) *and* E×B shear at the upper level of that observed experimentally in MAST, γ_E=0.9 c_s/a, where $\gamma_E = r/q \cdot \partial/\partial r(q/rB_{unit} \cdot \partial\Phi/\partial r)$ [11] and $c_s = \sqrt{T_e/m_i}$. For gradients representative of the MAST mid-radius ($a/L_{Te}=a/L_{Ti}=3$, $a/L_n=1$) $\gamma_E/\gamma_{lin,max} \sim 0.15$. (Similar ETG calculations using GS2 with E×B shear have recently been

achieved [10].) Simulations were performed in the collisionless and electrostatic limit. While β_e can be relatively large near the magnetic axis in MAST (β_e~0.1), previous ETG simulations for mid-radius parameters indicate the resulting *non-linear* transport is rather insensitive to the inclusion of EM perturbations [3].

The initial simulation domain uses a square perpendicular box $L_x=L_y=240\rho_e$, with 32 toroidal modes and 128 radial grid points, giving $k_\theta\rho_{e,max}\approx k_r\rho_{e,max}\approx 0.74$. The resolution in parallel orbit (10) and velocity space (128) use values sufficient to reach convergence and maintain entropy balance within ~5-10% [12]. Fig. 1(a) shows the time-averaged radial profile of χ_e for this case (black). As GYRO uses finite differences for the radial derivative, Dirichlet boundary conditions on fluctuating quantities (fixed at zero) are enforced when including profile variations (only ExB shear in these simulations). The effect is seen clearly in Fig. 1(a) as the transport is finite and flat in the interior but approaches zero at either radial boundary. In the absence of a source, this strong variation in transport will relax the effective equilibrium temperature gradient. To counteract this, boundary buffer zones [13] of finite width (Δ^b) are implemented that damp the axisymmetric components of the distribution function ($\sim\nu^b\cdot\delta f_{n=0}$), effectively acting as a local source. (A full-radius "adaptive source" [13,14] is not used here as there are no equilibrium profile variations.) Fig. 1(b) shows the radial profile of the time-averaged total effective gradient, $(a/L_{Te})_{total}$, for the buffer parameters used in the initial simulation ($\Delta^b=16\rho_e$, $\nu^b=1c_s/a$). It is clear that for these parameters there is a reduction of the effective gradient across the interior of the domain.

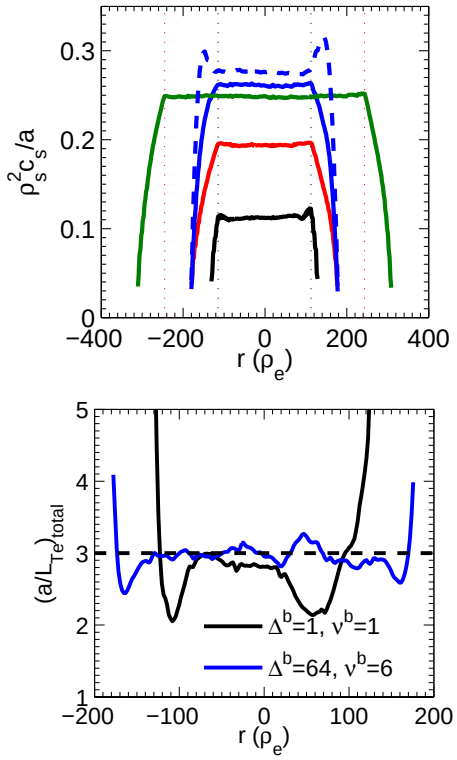

Fig. 1. (a) Profiles of χ_e from local GYRO simulations with E×B shear (non-periodic BCs) using different box widths, boundary widths, and boundary damping strength. (b) Effective electron temperature gradient profiles (including time-averaged $\langle\delta f_{n=0}\rangle_\theta$).

Fig. 1(a) illustrates the total transport increases as the buffer width and damping strength are increased (optimal parameters were previously determined for ion scale simulations, e.g. [14]). With ($\Delta^b=64\rho_e$, $\nu^b=6c_s/a$) the total effective T_e gradient remains near the input value (Fig. 1(b)). Fig. 2 shows the time-averaged value of χ_e vs. $(a/L_{Te})_{total}$ (averaged

over the interior of the domain) for a number of simulations that independently vary box size (black), buffer width (red), and damping strength (blue). With sufficiently large (Δ^b, ν^b) the transport is insensitive to further changes. As a consequence of the stiffness inherent in these ETG simulations, the transport increased almost threefold for a net increase in total effective gradient (in the interior) of only ~10%. The above exercise illustrates how sensitive the resulting transport can be to perturbations that modify the equilibrium gradients [14]; an effect that must be monitored in any numerical scheme using finite differences (non-spectral) in the radial direction with non-periodic boundary conditions (i.e., all global codes).

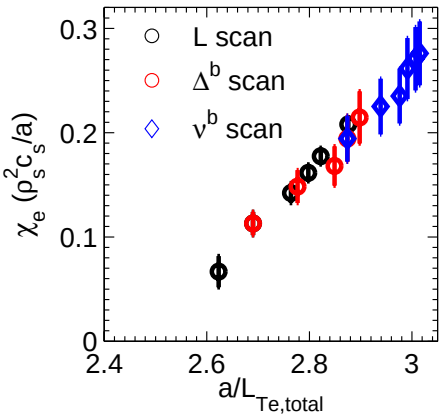

Fig. 2. Simulated transport χ_e vs. net effective T_e gradient for various simulations.

While the transport in the above simulations changed significantly for varying buffer parameters (total effective gradient), the resulting turbulence characteristics were largely unaffected. For instance, the spectra shape and correlation functions were nearly identical (correlation lengths at FWHM were $L_r \approx 3 \cdot L_y \approx 26\rho_e$).

Additional simulations demonstrate the transport is converged with respect to radial, parallel orbit and velocity space resolution. However, transport increases with binormal resolution up to $k_\theta \rho_{e,max}=1.5$ (for fixed box size). This is similar to the ETG-ai benchmark reported in [2], although here we have included both kinetic ions and finite E×B shear. While the binormal box size can be reduced a factor of two (i.e. half the number of toroidal modes) with no effect on saturation, this will likely depend on the level of E×B shear which does impact the low k_θ saturation. Fig. 3 shows the fractional transport spectra for the $L_x=L_y=240\rho_e$ box with $k\rho_{e,max}=0.74$ (black) and $k\rho_{e,max}=1.5$ (red), and a corresponding simulation with $L_x=2L_y=240\rho_e$, $k\rho_{e,max}=1.5$ (blue). The resulting transport reaches $\chi_e \approx 0.4\,\rho_s^2 c_s / a = 8\,\rho_e^2 v_{Te} / L_{Te}$ which is comparable to experimental values.

In neutral beam heated MAST discharges, the strong toroidal rotation ($Ma=v_{tor}/c_s \leq 1.0$, $c_s = \sqrt{T_e / m_i}$) and corresponding toroidal flow shear gives rise to the E×B shear included in the simulations above. In addition to this *perpendicular* E×B shear, *parallel* flow shear ($\gamma_P = qR/r \cdot \gamma_E$) should be included to consistently model the net *toroidal* flow shear. Fig. 4 shows the linear growth rates with and without the inclusion of toroidal flow and parallel

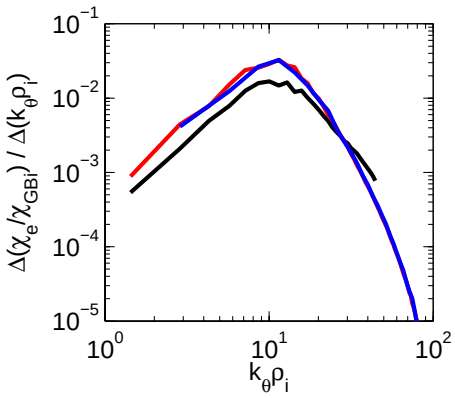

Fig. 3. Fractional transport spectra for simulations with different box sizes and binormal resolution.

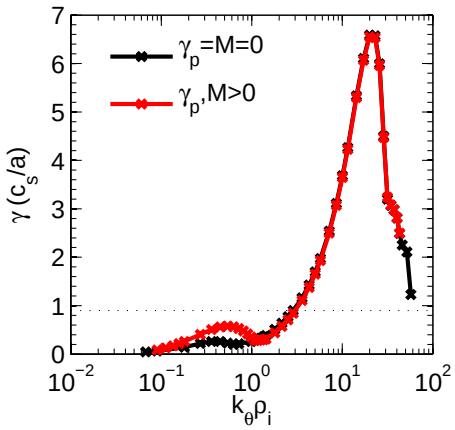

Fig. 4. Linear growth rates without (black) and with (red) finite toroidal flow and parallel flow shear.

flow shear (Ma=0.6, γ_P=4.0c_s/a). The addition of γ_P provides an additional linear instability drive (Kelvin-Helmholtz) evident in the $k_\theta\rho_i \leq 1$ growth rates. However, this increase is insufficient to overcome the E×B shear rate (dashed line) responsible for suppression of ion scale turbulence. It is not surprising that the resulting nonlinear ETG simulation ($k_\theta\rho_{i,min}$~1.5) is unaffected by the inclusion of finite Ma and γ_P at this radius.

The above simulations were performed in the local limit (flat profiles of n,T, and their gradients), which is reasonable when focusing only on electron scales (ρ_e/a~1/6000). However, measured ST profiles vary significantly over ion scales (ρ_i/a~1/100), including the gradients in n & T, toroidal flow and shear, as well as ε=r/R which impacts the parallel flow shear (q/ε) and particle trapping (~$\varepsilon^{1/2}$). Simulations using measured experimental profile variations are presently underway to access the impact of these variations on the resulting ion and electron scale transport in MAST.

Calculations were performed at the University of Warwick Centre for Scientific Computing and NERSC. This work was partly funded by the United Kingdom Engineering and Physical Sciences Research Council and by the European Communities under the contract of Association between EURATOM and UKAEA. The views and opinions expressed herein do not necessarily reflect those of the European Commission.

References

[1] A.R. Field *et al*., Proc. 20th IAEA Conf., Villamoura, EX/P2-11 (2004).
[2] W.M. Nevins *et al*., Phys. Plasmas **13**, 122306 (2006).
[3] N. Joiner *et al*., Plasma Phys. Control. Fusion **48**, 685 (2006).
[4] R.J. Akers *et al*., Proc. 22nd IAEA Conf., Geneva, EX/2-2 (2008).
[5] G.M. Staebler *et al*., Proc. 22nd IAEA Conf., Geneva, TH/P8-42 (2008).
[6] K.L. Wong *et al*., Phys. Plasmas **15**, 056108 (2008).
[7] D. Stutman *et al*., Phys. Rev. Lett. **102**, 115002 (2009).
[8] J. Candy & R.E. Waltz, J. Comput. Phys. **186**, 545 (2003).
[9] J. Candy, R.E. Waltz, C. Holland, M. Fahey, Plasma. Phys. Control. Fusion **49**, 1209 (2007).
[10] C.M. Roach *et al*., Gyrokinetic Simulations of Spherical Tokamaks, EPS, Sofia (2009).
[11] R.E. Waltz, G.D. Kerbel, J. Milovich, Phys. Plasmas **1**,2229 (1994).
[12] J. Candy & R.E. Waltz, Phys. Plasmas **13**, 032310 (2006).
[13] *GYRO Technical Guide*, J. Candy, http://web.gat.com/THEORY/images/e/ea/Gyro_technical_guide.pdf
[14] R.E. Waltz, J. Candy, M.N. Rosenbluth, Phys. Plasmas **9**, 1938 (2002).